Fatigue of Materials III: Advances and Emergences in Understanding
Edited by: T.S. Srivatsan, M. Ashraf Imam, and R. Srinivasan
TMS (The Minerals, Metals & Materials Society), 2014

CYCLIC STRAIN RESISTANCE, DEFORMATION AND FRACTURE BEHAVIOR OF A NOVEL ALLOY STEEL

K. Manigandan and T. S. Srivatsan
Division of Materials Science and Engineering
Department of Mechanical Engineering
The University of Akron
Akron, Ohio 44325-3903
E-Mail: tsrivatsan@uakron.edu

V. K. Vasudevan, D. Tammana and B. Poorbangi
School of Dynamic Systems
Materials Science and Engineering Program
University of Cincinnati
Cincinnati, Ohio 45221-0072
E-Mail: vijay.vasudevan@uc.edu

Abstract

In this paper, the results of a study on microstructural influences on cyclic strain response, deformation and fracture behavior of an alloy steel is presented Cyclic strain resistance exhibited a linear trend for the variation of both elastic strain amplitude with reversals-to-failure, and plastic strain amplitude with reversals-to-failure. Fracture morphology was observed to be the same at the macroscopic level over the entire range of cyclic strain amplitudes examined. However, at the fine microscopic level this alloy steel revealed fracture to be mixed-mode with features reminiscent of "locally" ductile and brittle failure mechanisms. The mechanisms governing strain response at the fine microscopic level, resultant fatigue life, and final fracture behavior are presented and discussed in light of the mutually interactive influences of intrinsic microstructural effects, deformation characteristics of the microstructural constituents during fully-reversed strain cycling, magnitude of cyclic strain amplitude, and resultant fatigue life.

Key Words: alloy steel, microstructure, tensile properties, fatigue

1. Introduction

The last four decades, i.e., since the early 1980's, manufacturers of all kinds of steels, spanning the domains of carbon steels, mild steel, stainless steels, alloy steels, tool steel and specialty steel have attempted to successfully engineer the use of these steels for a spectrum of applications spanning the domains of performance-critical and non-performance critical. This in turn has provided them with not only the required incentive but also the impetus to shift their attention and action towards the production, processing and use of new and improved high strength steels. The newer class of high strength steels is noted for their ability to offer an attractive combination of high tensile strength, acceptable fracture toughness, improved weldability coupled with acceptable performance in environments spanning a range of aggressiveness, to include both aqueous and gaseous, when compared one-on-one with the mild steel counterpart [1-10]. During the same time period production and processing of the family of new and improved high strength steels did culminate from progressive advancement of the processing and manufacturing techniques in the steel industry, particularly the domain of thermo-mechanical processing (TMP). In this connection, a control of heating and subsequent rolling process during production of the steel can result in the formation of a fine grain size end product.

The mechanical properties of the family of new and improved family of high strength steels are governed by the conjoint and mutually interactive influences of chemical composition, processing history, intrinsic microstructural features, temperature of operation, loading rate, and even potential constraints at the crack tip [11-20]. Conditions that are often favorable for minimizing crack tip constraints are also conducive for enhancing the ability of the candidate steel to be receptive to plastic deformation. This facilitates an overall improvement in fracture toughness coupled with an increased tolerance to fatigue damage at high temperatures. In more recent years, several studies have made an attempt to show the factors, ranging from: (i) an increase in part thickness, (ii) incorporation of engineering notches, (iii) increase in loading rate, and (iv) a lowering of the operating temperature, are often detrimental to both ductility and toughness of the steel [21-25].

In this paper, we present and discuss the results of a study aimed at understanding the influence of intrinsic microstructural effects on cyclic strain amplitude-controlled response; fatigue life and final fracture behavior of the high strength alloy steel Tenax^{TM} 310. The likely mechanisms governing cyclic strain resistance and resultant fatigue life, and final fracture behavior, are presented in light of the conjoint and mutually interactive influences of intrinsic microstructural effects, magnitude of cyclic strain amplitude, deformation characteristics of the microstructural constituents, and overall fatigue life.

2. Material

The high strength steel chosen for this study was Tenax^{TM} 310. This steel was provided by Carpenter Technology, Inc (based in Reading, PA, USA). The chemical composition (in weight percent) of the high strength alloy steel is given in **Table 1.** The presence of carbon in substantial amounts in this steel provides solid solution strengthening besides increasing hardenability through the formation, presence and distribution of alloy carbides. Presence of the

elements chromium (Cr) and molybdenum (Mo) results in the formation and presence of the second-phase particles chromium carbide (Cr_2C_3) and molybdenum carbide (Mo_2C), which are well dispersed through the microstructure. The carbide particles distributed through the microstructure contribute to enhancing strength of the steel matrix [26, 27]. The presence and distribution of a substantial number of such carbide particles in the microstructure is detrimental to both ductility and fracture toughness. This can be attributed to a 'local' increase in the number of sites that are easily susceptible to the early initiation of fine microscopic cracks. Presence of the element nickel (Ni) in the alloy steel helps in lowering the transition temperature thereby making the steel appropriate for use at low service temperatures. This steel, i.e.,Tenax^{TM} 310, also contains an appropriate amount of molybdenum, whose purpose is to refine the grain size besides forming molybdenum carbide (Mo_2C) and its indirect influence in contributing to enhancing both strength and impact toughness. This alloy steel was produced using the method of Arc VAR [VAR: Vacuum Arc Remelting); with Arc in this case being an initial arc-melt operation].

Table 1: Nominal chemical composition of Tenax ^{TM}310 (in weight percent)

Material	C	Mn	Si	P	S	Cr	Ni	Mo	Cu
Tenax ^{TM} 310	**0.401**	**0.63**	**2.03**	**0.004**	**<0.0005**	**1.26**	**3.76**	**1.01**	**0.53**

3. Experimental Procedures

3.1 Characterization of As-received Microstructure

A sample of the chosen high strength steel Tenax^{TM}310 was prepared very much in conformance with the standard procedures used for metallographic preparation of metal samples. The as-polished sample was then etched using nital reagent, i.e., a solution mixture of nitric acid in methanol. The polished and etched sample was subsequently examined in an optical microscope, at low magnifications, and photographed using standard bright field illumination technique.

Transmission electron microscopy (TEM) observations were used to investigate grain size, grain distribution, presence, size and distribution of the second-phase carbide particles and other fine intrinsic features in the microstructure of the as-provided material. Samples 0.5 mm to 0.6 mm in thickness were sliced from both the undeformed section [i.e. grip section] and deformed section (i.e. gage length) of the alloy steel test sample. From these slices were punched out thin discs having an effective diameter of 3-mm and a thickness of around 100 μm. The circular discs, referred to henceforth as samples, were dimpled using a dimpler machine [Model: FISCHIONE] and a diamond solution gradually down to 1 μm size. Using the technique of dimpling, the thickness of the sample was effectively reduced to around 20-30 μm. Subsequently, ion milling was used for the final stage of sample preparation for purpose of observation in a transmission electron microscope (TEM). Argon gas ion-milling was used with the gun angle set at 14 degrees and in a chamber that was cooled by liquid nitrogen. The resultant polished sample, referred to as a "thin-foil", was observed in a transmission electron microscope (Model: Phillips) operating at 200 kV.

3.2 Preparation of Test Specimen

Cylindrical test specimens, conforming to specifications outlined in ASTM E8 [28], were precision machined from the chosen steel. The threaded test specimens measured 59 mm in overall length and 6.35 mm in diameter at the thread section. The gage section of the machined test specimen measured 12.5 mm in length and 3.175 mm in diameter. The length-to-diameter ratio of the fatigue test specimen was chosen to ensure that it would not buckle under conditions of fully-reversed [R_ε = minimum strain / maximum strain ($\sigma_{minimum}$ / $\sigma_{maximum}$)] total strain amplitude-controlled cyclic deformation. To minimize the effects and/or contributions arising from both surface irregularities and surface finish, final preparation of the test specimen surface was achieved by mechanically polishing the gage section of all specimens using progressively finer grades of silicon carbide impregnated emery paper to remove any and all of the circumferential scratches and surface machining marks.

3.3 Mechanical Testing (Tension plus Fatigue)

Tensile tests were performed up until failure on a fully-automated, closed-loop servohydraulic mechanical test machine [INSTRON Model 8500 plus] equipped with a 10,000 kgf (98 KN) load cell. The test specimens were deformed at a constant strain rate of 0.0001/s. An axial 12.5 mm gage length extensometer was attached to the test specimen at the gage section, using rubber bands, to provide a precise measurement of strain during uniaxial loading and resultant stretching of the test specimen. All of the stress and strain measurements, parallel to the load line, were recorded on a PC-based data acquisition system [DAS].

The fatigue tests were also performed on a fully-automated closed-loop servohydraulic structural test machine. The tests were conducted in the axial total strain amplitude control mode under fully-reversed, push-pull, tension-compression loading. The test machine was aligned prior to the initiation of each fatigue test very much in conformance with the guidelines put forth by the manufacturer (INSTRON Corporation, Canton, MA, USA). For each individual test the test machine was programmed to maintain a constant nominal strain rate of 0.001/s. The test common signal (i.e., strain function) was a triangular waveform, and the mean strain was zero. All of the total strain amplitude-controlled ($\Delta\varepsilon_T/2$) cyclic fatigue tests were initiated in tension. A 12.7 mm clip-on extensometer was attached to the test specimen at the gage section, using rubber bands, for the purpose of monitoring total strain-amplitude ($\Delta\varepsilon_T/2$) during fully-reversed strain amplitude-controlled fatigue tests such that the magnitude of negative strain equals the magnitude of positive strain ($R_\varepsilon = \varepsilon_{min.}/\varepsilon_{max} = -1$). The controlled variable is total strain amplitude ($\Delta\varepsilon_T/2$) and the cyclic strain-controlled tests were performed over a range of total strain amplitudes ($\Delta\varepsilon_T/2$). The extensometer was calibrated prior to the initiation of each fatigue test. The tests were conducted at room temperature (27^o C) and in laboratory air environment (relative humidity of 55 percent). The stress and strain data for each fatigue test was recorded on a PC-based data acquisition system. The number of cycles-to-failure, or separation, is taken as fatigue life (N_f).

3.4 Analysis of Damage and Failure

The fracture surfaces of the cyclically deformed and failed fatigue test specimens of this alloy steel were comprehensively examined in a scanning electron microscope (SEM) to determine the following:
(i) the macroscopic fracture mode, and
(ii) characterize the fine scale topography, the nature of crack initiation, the extent and depth of early crack propagation, the extent and depth of stable crack propagation, and other intrinsic features on the fracture surface.
This was essential for establishing the microscopic mechanisms contributing to failure by fracture.

The distinction between the macroscopic mode and microscopic fracture mechanisms is based entirely on the magnification level at which the observations were made. The macroscopic mode referring to the overall nature of failure while the fine microscopic mechanisms being related to failure processes occurring at the "local or microscopic" level. This includes the following: (i) microscopic void formation, (ii) microscopic void growth and their eventual coalescence by way of impingement, and (iii) Nature, intensity and severity of the fine microscopic and macroscopic cracks dispersed through the fracture surface. The samples for observation in the scanning electron microscope (SEM) were obtained from the cyclically deformed and failed fatigue specimens by sectioning parallel to the fracture surface.

4. Results and Discussion

4.1 Initial Microstructure.

The optical microstructure of the chosen high strength steel is shown in **Figure 1.** The observed microstructure is typical of high strength steels in that it reveals a combination of carbon-rich and carbon-depleted regions. A higher carbon and alloy content in this high strength alloy steel results in a greater volume fraction of martensite in the carbon-rich regions. The presence and overall morphology of the martensite was much finer and intermingled with pockets of ferrite-rich regions, i.e., the carbon depleted region, in this high strength steel that was produced by vacuum arc re-melting (VAR). The presence of the hard, brittle and essentially elastic deforming martensite micro-constituent becomes a preferred site for high 'local' stress concentration during cyclic deformation. In addition to the presence of these two phases, or micro-constituents, i.e., ferrite and martensite, also dispersed through the microstructure were the alloy carbides. These particles result as a consequence of the alloy content in this high strength steel. The morphology of the martensite micro-constituent in the carbon-rich region is governed by a synergism of both chemical composition and processing technique, to include both primary processing and secondary processing that was used to engineer the starting material (Tenax^{TM} 310). These two phases along with the carbide particles exert an appreciable influence on cyclic fatigue response, fatigue life, nature of deformation and final fracture behavior, at the fine microscopic level, when specimen of the alloy steel is subject to cyclic loading.

Transmission electron microscopy observations of the thin foils taken from the undeformed alloy steel when viewed at low magnifications revealed a combination of elongated grains intermingled with the smaller grains. The grains were overall of varying size (**Figure 2a**). At the higher allowable magnifications of the TEM the observable and/or resolvable grains (**Figure 2b**) were oriented in the direction of mechanical deformation **(Figure 2c**).

4.2 Tensile Properties

The ambient temperature tensile properties of the candidate steel (Tenax^{TM}310) is summarized in **Table 2.** Results reported are the mean values based on duplicate tests. The elastic modulus of this steel is 194 GPa. The yield strength of this high strength alloy steel (Tenax^{TM} 310) is 1018 MPa and the ultimate tensile strength is 1225 MPa. The tensile strength is only marginally higher than the yield strength indicating the occurrence of slow degree of train hardening beyond yield. The ductility quantified by elongation over half-inch gage length was 14 percent. The reduction in test specimen cross-sectional area, another quantifiable measure of ductility, was 31 percent.

Table 2. A compilation of the room temperature tensile properties of the chosen steel

Material	**Elastic Modulus**		**Yield Strength**		**UTS**		**Elong.**	**Reduction in Area**
	Ksi	GPa	Ksi	MPa	Ksi	MPa	(%)	(%)
Tenax^{TM}310	**29747.2**	**205**	**147.7**	**1018.5**	**177.7**	**1225.4**	**13.4**	**31**

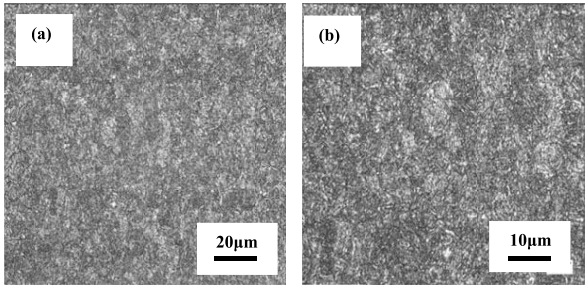

Figure 1. Optical micrographs showing the key micro-constituents present in alloy steel Tenax^{TM} 310 at two different magnifications.

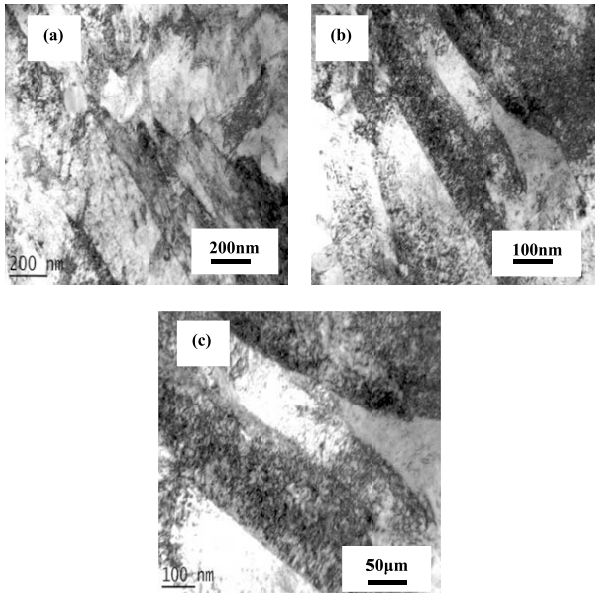

Figure 2. Transmission electron micrographs showing the size and shape of grains and their orientation.

4.3 Cyclic Strain-Controlled Fatigue Properties

A number of damaging processes are induced or caused by cyclic plastic strain. This often tends to affect not only the microstructure of this alloy steel, but also the cyclic strain resistance and resultant fatigue life [29-31]. The initiation and progressive growth of the damage through the microstructure of this alloy steel helps in relating the fatigue life (N_f) to cyclic strain amplitude [$\Delta\varepsilon$ /2] during fully-reversed [R_ε = -1] strain cycling. The relationship between plastic strain amplitude [$\Delta\varepsilon_P$ /2] and reversals-to- fatigue failure [$2N_f$], also known as the Coffin-Manson relationship, was determined for the LCF regime [$N_f < 10^4$ cycles] to be

$$[\Delta\varepsilon_P/2] = \varepsilon_f' [2N_f]^c \qquad [1]$$

The best straight line fit for the plastic strain amplitude [$\Delta\varepsilon_P$ /2] – reversals-to-fatigue life ($2N_f$) curve was obtained by linear regression analysis [29, 30]. An extrapolation of the best fit to the data points was made with the primary objective of determining the value of cyclic plastic strain amplitude ($\Delta\varepsilon_P$ /2) at $2N_f = 1$. This point in the plastic strain amplitude-fatigue life curve is referred to as the fatigue ductility coefficient [ε_f']. This coefficient provides a measure of cyclic ductility of the material. The slope of the plastic strain amplitude [$\Delta\varepsilon_P$ /2] -reversals-to-fatigue life ($2N_f$) curve gives the fatigue ductility exponent, **c**.

The effect of fully-reversed strain cycling on low cycle fatigue response of this alloy steel is shown in **Figure 3**. Variation of cyclic strain amplitude [$\Delta\varepsilon$ /2] with reversals-to-fatigue life [$2N_f$] curve can be viewed as an indication of the resistance offered by the microstructure of this alloy steel to both crack initiation and failure under conditions of fully-reversed strain cycling. Throughout strain-controlled testing of this alloy steel, over the range of strain amplitudes studied, there was no indication of the occurrence of specimen buckling. Based on width and height of the hysteresis loop for the different cycles, the plastic strain, elastic strain and stress amplitude values were recorded by the control unit of the servohydraulic test machine (INSTRON Model 8500 Plus) For the chosen orientation of this alloy steel the variation of elastic strain amplitude [$\Delta\varepsilon_e$ /2] with reversals-to-fatigue life [$2N_f$] is linear and the Basquin relationship is satisfied.

$$[\Delta\varepsilon_e/2] = \{\sigma_f' / E\} [2N_f]^b \qquad (2)$$

Variation of plastic strain amplitude [$\Delta\varepsilon_P$ /2] with reversals-to-fatigue life [$2N_f$] was also linear and the Coffin Manson relationship is satisfied and can be used to determine the fatigue behavior in the strain-controlled LCF regime [$N_f < 10^4$ cycles]. The value of fatigue ductility exponent [c] is 0.22. This value is well within the generally observed range of 0.2 to 0.7 for most metals and their alloy counterparts [29-31].

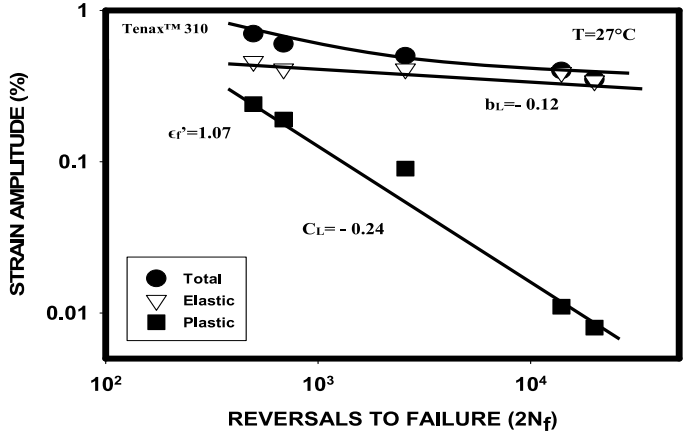

Figure 3. Variation of cyclic strain amplitude ($\Delta\varepsilon/2$) with reversals- to-failure ($2N_f$) for alloy steel Tenax^{TM}310 at room temperature (27^o C).

4.4 Cyclic Stress Response

The cyclic stress response curves exemplify the variation of cyclic stress amplitude ($\Delta\sigma$ /2) with cycles (N), at a fixed strain amplitude [$\Delta\varepsilon_T$ /2]. These curves concurrently provide a lucid illustration of the path taken by this alloy steel to its final level of stress during fully-reversed total strain amplitude-controlled cyclic deformation. The curves also provide useful

information pertaining to the overall cyclic stability of the chosen alloy steel. Stability of the intrinsic microstructural features, during fully-reversed strain cycling, in conjunction with an ability of the microstructure of this high alloy steel to distribute the plastic strain over the entire microstructural volume are factors that govern both the stress response and resultant fatigue life (N_f). Details of the nature of stress response, stress versus strain response and microscopic mechanisms governing the stress-strain response of this alloy steel can be found elsewhere [32].

4.5 Cyclic Fracture Behavior

At room temperature (27^{o}C) fracture surfaces of the samples that were cyclically deformed at both high cyclic strain amplitude and resultant short fatigue life and low cyclic strain amplitude and concomitant long fatigue life reveal near similar topography at the macroscopic level. At the fine microscopic level the fracture surface features were found to vary with cyclic strain amplitude and resultant fatigue life. Representative fractographs of the fatigue fracture surface are shown in **Figures 4-7.**

4.5.1 High Cyclic Strain Amplitude (1.0 pct.) [Fatigue Life = 1,292 cycles]

At this value of total strain amplitude (1.00 pct.) and resultant fatigue life of 1,292 cycles macroscopic fracture of this alloy steel specimen was essentially normal to the far-field stress axis (**Figure 4a).** Macroscopic or low magnification, observation in the scanning electron microscope (SEM) revealed the region of crack initiation and early microscopic crack growth to be smooth and inlaid with an array of fine microscopic cracks intermingled with macroscopic cracks (**Figure 4 b**). The region of stable crack growth prior to overload fracture surface was microscopically rough (**Figure 4 c**). At higher allowable magnifications of the scanning electron microscope this region revealed a combination of microscopic cracks, voids and dimples. These fine microscopic features are reminiscent of both brittle and ductile failure mechanisms occurring at the fine microscopic level. The region of unstable crack growth prior to overload revealed a microscopically rough fracture surface with cracking along the grain boundaries and grain boundary triple junctions (**Figure 5a**). The region of overload revealed a sizeable population of dimples of varying size indicative of locally acting ductile failure mechanisms **(Figure 5b).**

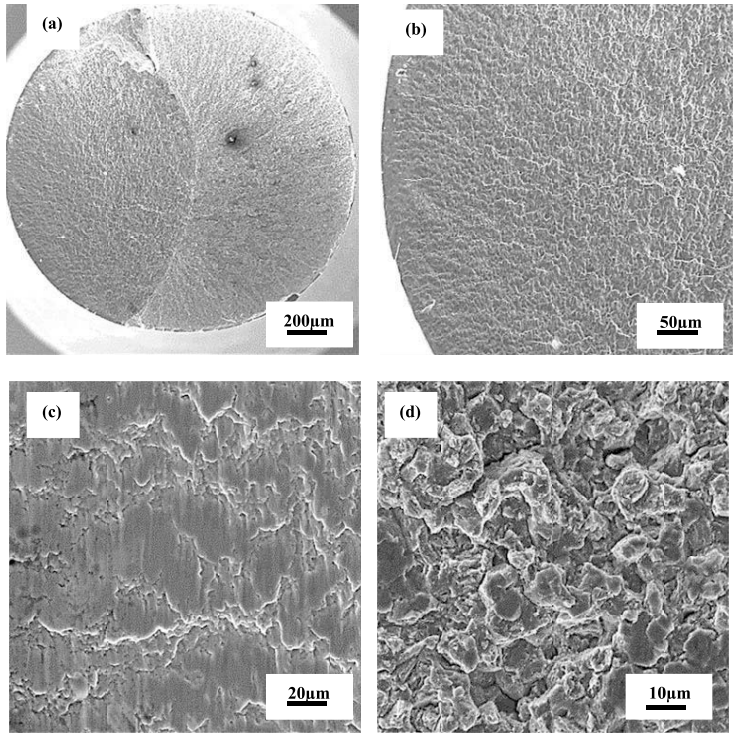

Figure 4. **Scanning electron micrographs of the fatigue fracture surface of alloy steel Tenax™ 310 sample, cyclically deformed at a strain amplitude of 1.00%, with a fatigue life of 1,292 cycles, showing:**

- **(a) Overall morphology of failure**
- **(b) High magnification observation of (a), Microscopically rough**
- **(c) Microscopic cracks in the region of crack initiation and early crack growth**
- **(d) Region of stable crack growth: microscopically rough**

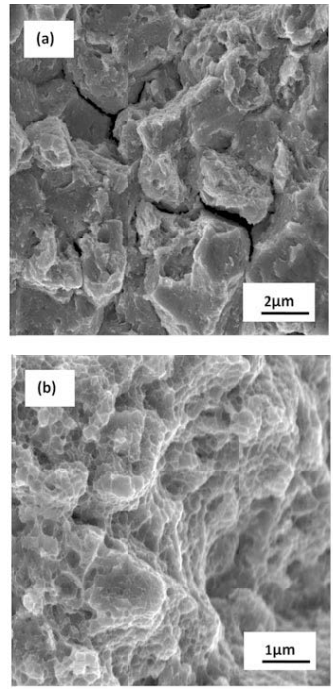

Figure 5. **Scanning electron micrographs of the fatigue fracture surface of alloy steel Tenax™ 310 sample, cyclically deformed at a strain amplitude of 1.00% with a fatigue life of 1,292 cycles, showing**

(a) Region of unstable crack growth showing cracking along the grain boundaries.

(b) Population of dimples covering the overload fracture surface.

4.5.2 Cyclic Strain Amplitude of 0.80 percent [Fatigue life = 6,992 cycles].

At this lower total strain amplitude of 0.80 pct. and resultant fatigue life of 6,992 cycles, overall morphology was normal to the far-field stress axis revealing two distinct regions representing fatigue and overload **(Figure 6-a**). The transition region (**Figure 6-b**) between fatigue and overload was rough at the microscopic level comprising of a population of fine microscopic cracks reminiscent of brittle mechanisms occurring at the fine microscopic level (**Figure 6-c**). At higher magnification this region of the fracture surface revealed a noticeably array of fine microscopic cracks intermingled with macroscopic cracks (**Figure 6-d).** The region of early microscopic crack growth was noticeably flat and covered with not easily discernible striation-like features coupled with isolated macroscopic cracks. Both these features are clearly indicative of both ductile and brittle mechanisms occurring at the fine microscopic level (**Figure 7-a**). The region of unstable crack growth immediately prior to overload was rough with isolated pockets of striations and featureless transgranular pockets that were intermingled with fine microscopic cracks (**Figure 7-b**).

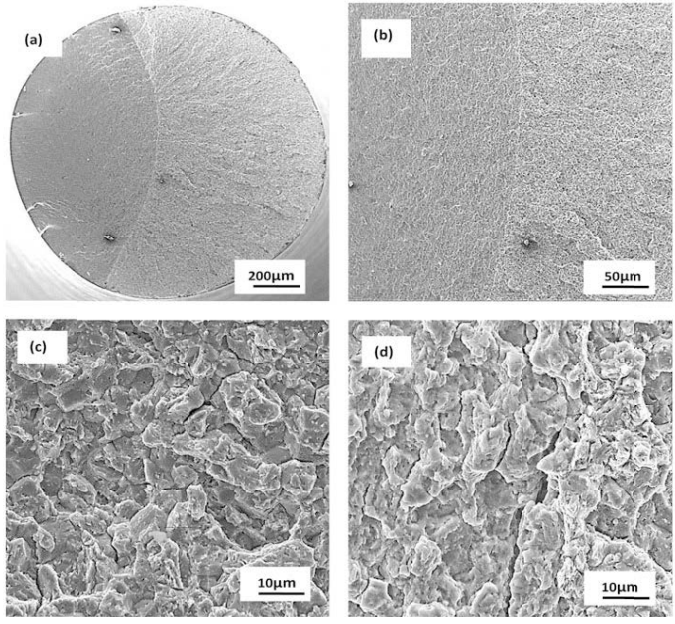

Figure 6. **Scanning electron micrographs of the fatigue fracture surface of alloy steel Tenax™ 310 sample, cyclically deformed at a strain amplitude of 0.80%, with a fatigue life of 6,992 cycles, showing:**

- **(a) Overall morphology showing distinct regions of fatigue and overload**
- **(b) The transition region microscopically rough**
- **(c) Fine microscopic cracks on the fatigue fracture surface prior to onset of overload**
- **(d) High magnification observation of the region of unstable crack growth reveals both microscopic and macroscopic cracks.**

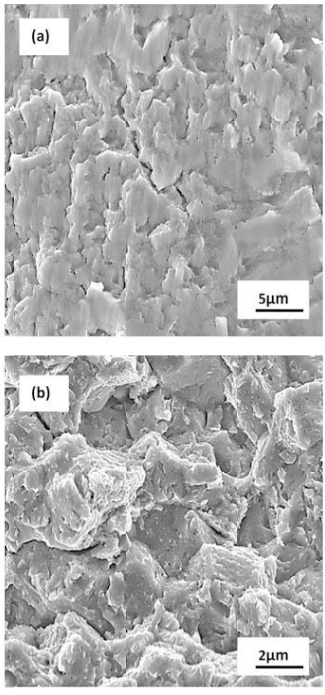

Figure 7. **Scanning electron micrographs of the fatigue fracture surface of alloy steel Tenax^{TM} 310 sample, that was cyclically deformed at strain amplitude of 0.80 pct., with a fatigue life of 6,992 cycles, showing:**
(a) The region of early microscopic crack growth flat and covered with isolated microscopic cracks.
(b) **Isolated pockets of striations and transgranular pockets in region of unstable crack growth**

4.6 Mechanisms Governing Cyclic Deformation and Fracture Behavior

Under conditions of fully-reversed strain cycling at room temperature (27^{o} C) the mechanisms controlling fracture of this alloy steel can be summarized as follows:

(i) An observable mismatch in strain carrying capability between the soft, ductile and plastically deforming matrix of alloy steel Tenax^{TM}310 and the hard, brittle and essentially elastically deforming microstructural feature, be it the martensite micro-constituent or coarse second-phase carbide particle.

(ii) This causes a large concentration of stress to occur at both the second-phase carbide particle and martensite micro-constituent, thereby enabling in cracking to occur at its interface with the soft metal matrix. The ease of occurrence of fine microscopic cracks suggests that 'local' plastic strain dominates in regions of the hard, brittle and essentially elastically deforming microstructural feature.

Cracking of both the martensite micro-constituent and the coarse second-phase carbide particles occurs normal to the far-field stress axis. The occurrence of plastic strain inhomogeneity at the fine microscopic level (**Figure 8**) within the grains coupled with the presence of coarse second-phase carbide particles is responsible for the traces of intergranular cracking observed.

The fine microscopic mechanisms, which tend to control the variation of cyclic stress amplitude with cycles (N) during fully-reversed strain cycling of this high strength low alloy steel Tenax 310 are dependent on the intrinsic influence of microstructural features and the cyclic strain range. The most likely mechanisms contributing to governing stress response of this high strength alloy steel Tenax ^{TM} 310 can be ascribed to the concurrent and mutually interactive influences of the following events

.

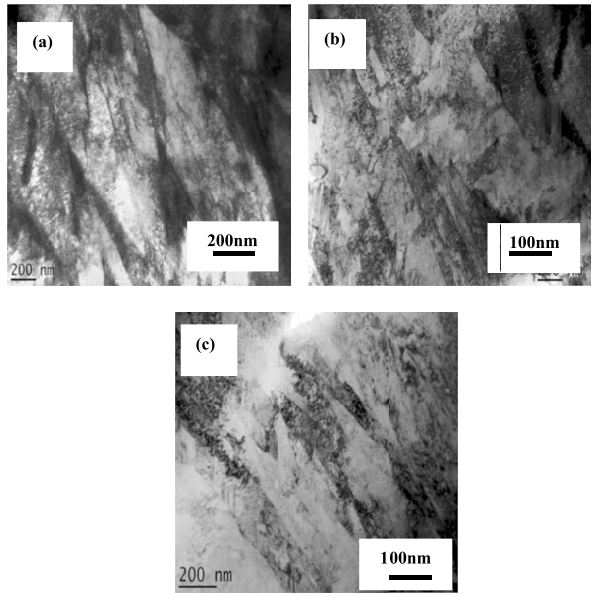

Figure 8: **Transmission electron micrographs showing the nature and deformation in test sample that was cyclically deformed at strain amplitude of 1.0 pct. with fatigue life of 1292 cycles.**

(a) A gradual increase in the density of dislocations present in the microstructure of this low alloy steel, during fully-reversed cyclic deformation in the plastic range, by the process of dislocation multiplication.

(b) Dislocation-dislocation interactions arising as a direct consequence of an increase in the interaction of a moving dislocation with other dislocations.

(c) An interaction of the moving dislocations with the second-phase constituents i.e., the carbide particles, dispersed through the microstructure coupled with the formation and presence of fine slip bands and their impingement on grain boundaries and resultant stress concentration

The dislocation-dislocation interactions coupled with an interaction of the moving dislocations with the microstructural constituents and grain boundaries is responsible for the hardening or strengthening that occurs at the fine microscopic level during fully reversed cyclic deformation. When the local stress concentration (σ^*) caused by the gradual build-up of dislocations at a second-phase particle exceeds a critical value (σ_C^*), microscopic crack initiation is favored to occur through rupture of the hard, brittle and essentially elastically deforming second-phase particle. With continued cyclic straining the fine microscopic cracks that were easily initiated gradually propagate through the microstructure and eventually link to form one or more macroscopic cracks. The early initiation of fine microscopic cracks coupled with their concurrent growth through the microstructure of this alloy steel and culminating in their eventual linkage upon continued cyclic straining results in a noticeable decrease in stress carrying capability of the microstructure, eventually culminating in failure by fracture.

5. Conclusions

Results of an investigation on understanding the influence of strain cycling on mechanical response, deformation and fracture behavior of an alloy steel, i.e., Tenax TM 310, provides the following key findings.

1. Optical microstructure of this alloy steel revealed a combination of carbon-rich, alloy-rich and carbon-depleted regions. The presence of both carbon and alloy content in this steel resulted in the presence of a noticeable volume fraction of second-phase particles and martensite micro-constituent in the alloy-rich and carbon-rich regions.

2. The elastic modulus of this alloy steel is 205 GPa. The yield strength is 1019 MPa and the ultimate tensile strength is 1225 MPa. The higher tensile strength indicates the occurrence of strain hardening beyond yield. The ductility quantified by elongation over 0.5 inch (12.7 mm) gage length was 13.4 pct. The reduction in test specimen cross-section area was 31 pct.

3. This alloy steel exhibited a linear trend for the variation of elastic strain amplitude ($\Delta\varepsilon_e/2$) with reversals-to-failure ($2N_f$), and plastic strain amplitude ($\Delta\varepsilon_P/2$) with reversals-to-failure ($2N_f$), in conformance with the behavior shown by other alloy steels and carbon steels.

4. Fracture morphology was about the same at the macroscopic level over the entire range of cyclic strain amplitudes examined. At the fine microscopic level the alloy steel test specimen that was deformed at the higher cyclic strain amplitude revealed fracture to be mixed-mode, i.e., a combination of ductile and brittle features. At the lower strain amplitude, microscopic observations of the fracture surface revealed predominantly ductile, i.e., a population of fine microscopic voids intermingled with dimples, with only traces of brittle failure mechanisms.

References

1. J.S. Pascover and S.J. Matas: Structure and Properties of Ultra-High Strength Steels, ASTM STP 370, ASTM, Philadelphia, USA, 1965, p. 370.

2. A. J. Baker, E. J. Laura and R. P. Wei in Structure and Properties of Ultrahigh Strength Steels, ASTM STP 370, ASTM,Philadelphia, PA, 1965, p. 3.

3. Strength Materials (edited by V.F. Zackay) John Wiley and Sons, New York, USA, 1965, p. 199,

4. B. R. Banerjee., Structure and Properties of Ultrahigh Strength Steels, ASTM, STP 370, ASTM, Philadelphia, PA, 1965, p. 94.

5. G.E. Pellissier**: Engineering Fracture Mechanics**, 1968, Vol. 1, pp. 55-65.

6. John R. Lowe, Jr.: **Engineering Fracture Mechanics**, 1969, Vol. 1, pp. 55-65.8

7. V.F. Zackay, E.R. Parker, R.D. Goolsby and W.E. Wood: **Nature** Physical Science, 1972, Vol. 236, No. 68, pp. 108-115.

8. D. Huang and G. Thomas: **Metallurgical Transactions**, 1972, Vol. 2, p. 1587

9. R.O. Ritchie, B. Francis and W.L. Server: **Metallurgical Transactions**, 1976, Vol. 7A, pp. 831-841.

10. J.L. Youngblood and M. Raghavan: **Metallurgical Transaction**, Vol. 8A, 1977, pp. 1439-1445.

11. G.Y. Lai, W.E. Wood, R.A. Clark, V.F. Zackay, E.R. Parker, **Metallurgical Transactions**. 5 (1974), 1663–1670.

12. G.Y. Lai, **Materials Science Engineering**, 19 (1975) 153–156.

13 F. Zia Ebrahimi, G. Krauss, **Metallurgical Transactions** 14A (1983) 1109–1119.

14. M. Sudo abd T. Iwai: **International Journal of ISIJ**, Vol. 23, 1983, pp. 284-302.

15 M. Sudio, S. Hashimoto, S. Kambe: **International Journal ISIJ**, Vol. 23, 1983, pp. 303-311.

16 F. Zia Ebrahimi, G. Krauss, **Acta Metallurgica**. 32 (1984) 1767–1777.

17. I. Kim, S. Rachel and W. Dahl: Steel Research, Vol. 58, 1987, pp. 186-190.

18. B.Y. Choi, G. Krauss, D.K. Matlock, Bainite formation and deformation behavior in an intercritically annealed Fe-1.0Mn-0.09C steel, **Scripta Metallurgica**, Vol. 22, 1988, pp. 1575-1580.

19. B.C. Kim, S. Lee, D.Y. Lee, N.J. Kim, **Metallurgical Transactions,** 22A (1991) 1889–1892.

20. D.K. Matlock and G. Krauss, Observation of deformation and transformation behavior of retained austenite in a 0.14C-1.2Si-Mn steel with ferrite-bainite-austenite structure, **Materials Science and Engineering A**, Volume 165, Issue 1, 25 June 1993, pp 1–8

21. Application of Fracture Toughness Parameters to Structural Metals, edited by Herman Greenberg, Gordon and Breach, New York, USA, 1966.

22. R.O. Ritchie, B. Francis, W.L. Server, **Metallurgical Transactions,** 7A (1976) 831–838.

23. W.E. Wood, **Metallurgical Transactions**, 8A (1977) 1195–1199.

24. R.O. Ritchie, R.M. Horn, **Metallurgical Transactions**, 9A (1978), pp. 331–341.

25. B.V. Narasimha Rao, G. Thomas, **Metallurgical Transactions**, 11A (1980) 441–457.

26. D. Thomas, D. Schmatz and W.W. Gerberich: in High Strength Materials (Edited by: V.F. Zackay) John Wiley and Sons, New York, USA, 1965, pp. 199-209

27. R. Hertzberg, Deformation and Fracture Mechanics of Engineering Materials, Second Edition, John Wiley and Sons, 1983,

28. ASTM E-8-06: Tensile Testing of Metallic Materials, American Society of Testing and Materials, Philadelphia, PA, 2006.

29. L. F. Coffin, Jr., and J.F. Travernelli: "The Cyclic Straining and Fatigue of Metals", **Transactions TMS-AIME**, Vol.215 (5), pp. 794-806.

30. S.S. Manson, and M. H. Hirschberg, "Fatigue Behavior of Strain Cycling in the Low and Intermediate Cycle Range," 10th Sagamore Army Materials Research Conference, Raquette Lake, NY, August 13-16, 1963.

31. T. H. Topper, B. I. Sandor, and J. Morrow, "Cumulative Fatigue Damage Under Strain Control" Journal of Materials, Vol. 4, 1969, pp. 189-199.

32. S. S. Manson: NASA Technical Note, National Aeronautics and Space Administration, 1954, pp 2933 - 2940.

33. K. Manigandan, and T. S. Srivatsan: **Journal of Strain Analysis for Design (**in review) 2014.

Acknowledgements

The authors (**TSS and KM**) extend most sincere thanks and overwhelming appreciation to **Carpenter Technology Corporation** (Reading, PA, USA: Program, Manager: ***Mr. Michael Schmidt***, Technical Director: ***Dr. Timothy Anderson***) for providing both material and financial support that made this research endeavor possible.